

Single-Electron-Spin Measurements in Si-Based Semiconductor Nanostructures

H.W. Jiang¹, E. Yablonovitch¹, M. Xiao¹, M. Sakr¹, G. Scott¹, and E.T. Croke²

¹ University of California, Los Angeles, CA 90095, USA

² HRL Laboratories, LLC, Malibu, CA 90265, USA

Abstract. In this chapter, we review the experimental efforts that focus on the measurement of single-electron spins in two particular Si-based semiconductor nanostructure systems. First, we describe experiments in a real transistor structure (i.e., a submicrometer commercial Si field effect transistor) in which the source/drain channel is used to electrically detect the spin states of an adjacent single paramagnetic spin center. This transistor structure is similar to a number of proposed spin-based qubit architectures that can be used as a potential quantum information processor. Second, we describe the effort to fabricate similar devices in specially designed semiconductor structures that promise greater control over electron spin, the ability to entangle two spins, and to eventually build a scalable quantum processor. In these engineered structures, quantum dots are created by metallic gates patterned over a 2D electron gas in a strained silicon-germanium heterostructure. In addition to the discussion of fabrication issues, we also show examples of single-electron-spin measurements in the few-electron regime of quantum dots.

1 Introduction

Isolated electron spins in low-temperature semiconductors are now recognized to have considerable potential for storing and manipulating quantum information. One of the attractions of a spin in a semiconductor is its very long decoherence time. The tunable spin-orbital coupling and the ability to control the electron wavefunctions in semiconductors allow gate operations on the spins. Another advantage is that they can be embedded into transistor structures, a premise that lends itself to the large-scale integration necessary for a quantum information processor. The extensive collection of chipmaking techniques, accumulated over decades, is expected to be extremely invaluable for building such a scalable processor. Possible applications of the quantum information processing devices including encryption and secure communications are recognized to be important to a modern society. While a fully functional factorization engine needs at least 1000 quantum logic bits, communication devices such as a quantum repeater require only 3 quantum logic gates [1].

Amongst various semiconductor materials, silicon is recognized to be a leading candidate for this purpose [2]. Electron spins in Si are endowed with the particular properties that would make them useful as qubits. The most important property is the safe preservation of quantum-mechanical phase information. It has been demonstrated experimentally that isotopically pure Si materials can have extremely long phase-coherence times, many orders of magnitude longer than that for group III–V semiconductors [3]. The primary mechanism for electron-spin decoherence of electron-spin states is their interaction with nuclear spins. If the nuclear spins sense, in any way, the relative up and down orientation of the electron spin, they become entangled with the electron-spin Zeeman levels, destroying the quantum coherence. It is fortunate that silicon is 95 per cent nuclear-spin free, and that germanium is 92 per cent nuclear-spin free. They are both subject to additional isotopic purification. Isotopically pure epitaxial Si²⁸ is 99.9 per cent nuclear-spin free, and is commercially available, while the III–V semiconductors have no spin-zero nuclei. In addition, Si can be embedded in strained silicon-germanium heterostructures. In strained SiGe structures, spin-orbital coupling is tunable, which makes gate operations on an individual spin possible [4].

Several schemes for measuring the electron spin in compound semiconductor structures have been proposed for quantum information processing [4–6]. In order to physically implement any of the proposals, it is essential to measure the state of a single spin. Diverse ideas for electrical detection of the state of an isolated spin have been discussed, however, all of them present significant experimental challenges.

In this chapter, we review the experimental efforts that focus on the measurement of single-electron spins in two particular Si-based semiconductor nanostructure systems. First, we will describe experiments in a real transistor structure (i.e., a submicrometer commercial Si field effect transistor) in which the source/drain channel is used to electrically detect the spin states of an adjacent single paramagnetic spin center. This transistor structure is similar to a number of proposed spin-based qubit architectures that can be used as a potential quantum information processor. Secondly, we will describe the effort to fabricate similar devices in specially designed semiconductor structures that promise greater control over electron spin, the ability to entangle two spins, and to eventually build a scalable quantum processor. In these engineered structures, quantum dots are created by metallic gates patterned over a 2D electron gas in a strained silicon-germanium heterostructure. As has been mentioned, SiGe is expected to be a superior material compared to III–V semiconductors for scalable quantum information processors. In addition to the discussion of fabrication issues, we will also show examples of single-electron-spin measurements in the few-electron regime of quantum dots.

2 Measurements of a Single Spin in the SiO₂ of a Submicrometer Si Field Effect Transistor

For the single-spin measurements, a sequence of submicrometer n-channel Si field effect transistors (FETs) have been used. It is well known from the extensive literature of magnetic-resonance studies that there exist structural paramagnetic defects near the Si/SiO₂ interface. For a small device, it is possible that there is only one isolated trap state that is both within the tunneling distance of the channel, and with an energy that is close to the Fermi level.

Figure 1a shows a microscope picture of a typical Si FET sample used for the single-spin measurements. It shows a line of devices on the left, and a magnified view of a single device on the right. The device has a channel size of length 300 nm by width 270 nm. Figures 1b and c sketch a simplified version of such a device that represents the two charged states of the trap in the experimental system. In a FET, the conductivity of a “channel” from the drain to the source is controlled by a voltage applied to the gate.

For the FET device, the signature of a single trap state is the current switching between two discrete states, known as the random telegraph signal (RTS). Over the years, observations of RTS, have been reported in a variety of mesoscopic electronic systems. It has now been commonly accepted that the RTS is an unequivocal signature of capture and emission of one electron

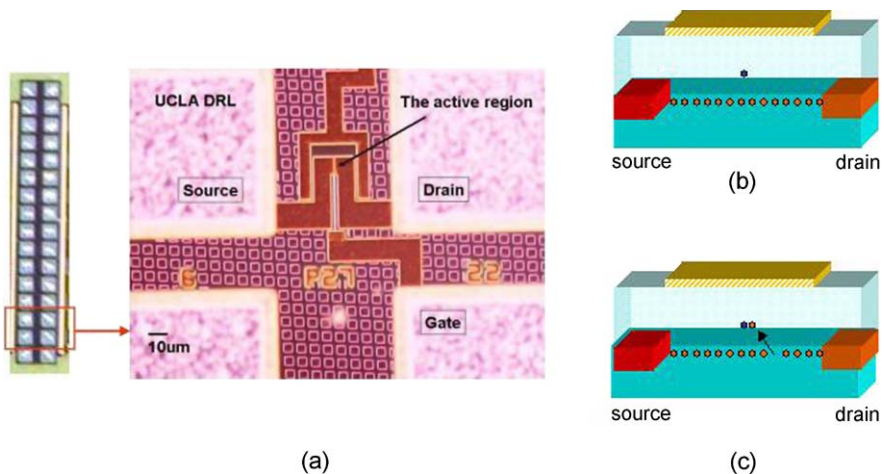


Fig. 1. (a) Microscope picture of a typical Si field effect transistor device used for the single-spin measurements. It shows a line of devices on the *left*, and a magnified view of one device on the *right*. The *light squares* are the contact surfaces. The device has a channel length of 300 nm and a channel width of 270 nm. (b) The two charge states of a trap in the SiO₂ of the device located in the close proximity of the channel

by a single trap state.¹ In particular, the pioneering work of Ralls et al. [8] demonstrated that, for a MOSFET, when the Fermi level of the conducting channel is in the proximity of the trap energy level, the electron from the channel can tunnel on and off the trap. Changes in the trap charge state directly affect the Coulomb scattering rate for carriers, thus producing jumps in electrical current. For small-size devices at low temperatures, there is often only one defect within $k_B T$ of the Fermi level. Therefore, the electrical signal is insensitive to the other traps. The traps in a FET are normally very stable defects, as the measurements are reproducible over many thermal cycles from room temperature to cryogenic temperatures.

2.1 Statistical Measurements

In the rich literature of RTS, work has focused predominantly on the electrical properties of the trap in the absence of a magnetic field. The essential ingredient for detecting a single spin-flip is to convert the spin orientation of the trap to an electric charge. Here, by analyzing the change of statistics of the RTS in the magnetic field, we show that the RTS is an effective measurement to probe the spin state of the trap [9].

In the single-spin measurement experiments, the channel current can be recorded by a fast dynamic signal analyzer or by a high-frequency lockin amplifier. In Fig. 2a the channel current is recorded over a narrow gate voltage ramped from 720 mV to 760 mV, swept in a 10-ms time interval. Actually, 80 per cent of the transistors that we tested had no such trap states at all. In those cases, we can apply a high-voltage spike to the gate to induce a paramagnetic defect, with hot electrons, for study. Superimposed on the monotonically increasing background source/drain current is stochastic switching between two discrete values of channel current. This switching is the above-mentioned well-known RTS, which is a hallmark of the capture and emission of one electron by a single trap state. The well-defined RTS evolution demonstrates that over the 720 mV to 760 mV range, the trap is energetically well isolated from other traps. A filled trap implies electrostatic repulsion that diminishes the channel current. At high gate voltages (near point C in Fig. 2a) the Fermi level, E_F , is well above the trap level, E_T . Thus, the trap is almost always filled, repelling electrons and allowing less current to flow in the source/drain channel. In contrast, at low gate voltages (near point A in Fig. 2a), when E_F is well below E_T , the trap is empty most of the time and the high current state is more probable. At the midpoint, when $E_F = E_T$ (near point B in Fig. 2a), the probability for the trap filling is about 50 per cent. Thus, the source/drain current senses the two charge states of the trap.

In this experiment the FET channel is basically a very sensitive electrometer. A fast dynamic analyzer allows one to collect the data in real time with

¹ For a comprehensive review, see [7].

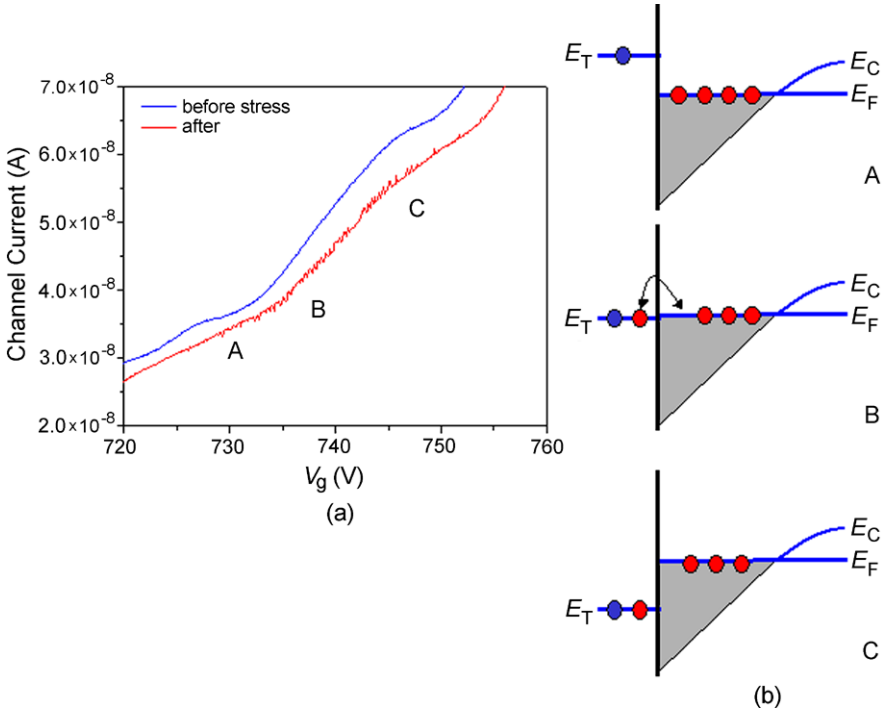


Fig. 2. (a) The channel current is measured as a function of the gate voltage with a constant scanning rate of about mV/ms, at 4.2 K before and after the electric stress. The evolution of the change in trap-filling probability can be seen after the stress. (b) The energy diagram of the single trap and FET channel bath for the points A, B, and C of curve displayed in (a). Here, the singly occupied state should actually be downshifted by the Coulomb correlation energy, U , not shown for simplicity

a maximum rate of several hundred kHz. The frequency of the tunneling from the channel to the trap for this particular sample is about 20 kHz. Thus, the charge sensitivity of the small FET channel is of the order of $10^{-4} e/(\text{Hz})^{1/2}$. The rapid tunneling rate also allows us to obtain excellent statistics of the trap-filling probability in a short period of time, which is necessary for detecting the small change in statistical distribution at ESR (discussed later).

Here, we would like to describe briefly how one can compute the RTS statistics through a simple and reliable method using histograms. Figure 3 shows the histograms for varying gate voltages. For each gate voltage, the histogram for the channel current shows two Gaussian distributions, corresponding to the two current levels. Without any noise, a histogram should consist of two discrete lines positioned at the two discrete levels. White noise spreads out the two lines to two overlapping Gaussian distributions. Figure 3 shows that the left peak grows while the right peak diminishes for increasing gate voltage. This is consistent with the fact that the defect is gradually charged. The

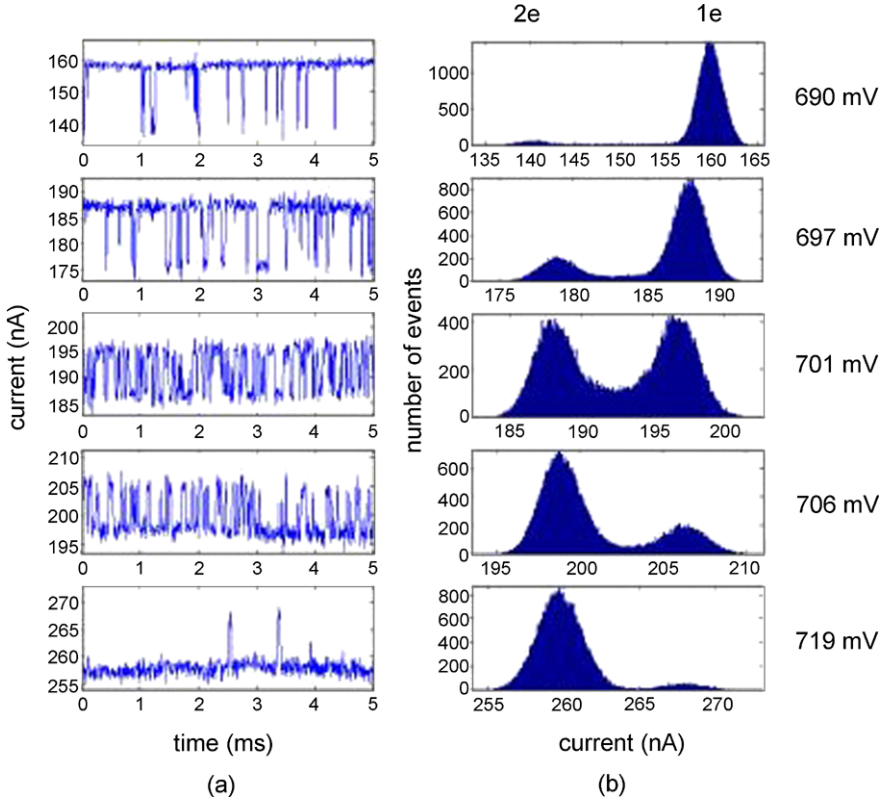


Fig. 3. (a) Channel current as a function of time for varying gate voltages at 4.2K. The data is displayed only for 5ms. From *top to bottom*, V_g is 690, 697, 701, 706 and 719 mV. (b) Histograms of RTS. Each histogram consists of two Gaussian distributions, corresponding to the two current levels. As V_g goes up, the peak for the low-current state dominates over the other one

ratio of the lifetimes on the high and low current states is the ratio of the area under the left peak to the area under the right peak. A routine can be used to automatically fit the histogram with two Gaussian distributions. Then, the area under each peak can be obtained easily.

The Zeeman shift of the single trap can be readily identified by studying the trap energy shift of the 50:50 trap-filling-probability point (where the Fermi Level E_F lines up with the trap energy E_T) as a function of magnetic field. Figure 4a shows the Zeeman shift of this 50:50 trap-filling energy as a function of an inplane magnetic field. The trap energy shift was inferred from the gate voltage shift [9].

Based on the sign of the Zeeman shift, we show that the charging transition transfers from a single-charge state, 1e, to a double-charge state, 2e; i.e., the charging is 1 to 2 rather than 0 to 1. In the energy diagram, Fig. 4b,

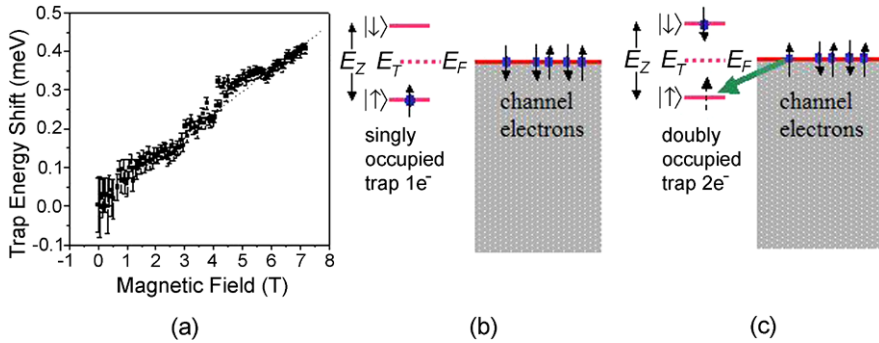


Fig. 4. (a) At the 50:50 trap-filling-probability point, the Fermi level matches the available defect energy level. The positive Zeeman shift of the trap energy versus magnetic field implies a $1e$ to $2e$ transition in the defect, rather than a $0e$ to $1e$ transition. (b) The Zeeman-split trap level relative to the FET channel Fermi level. The Fermi level would have to shift toward the upper Zeeman level to reach 50:50 occupation probability. (The singly occupied state should actually be downshifted by the Coulomb correlation energy, U , not shown.) (c) If the spin flips, the lower Zeeman level can become filled, producing the doubly occupied trap

the empty trap is modeled as an unpaired electron (e.g., a dangling bond) that occupies the level E_T (the central dashed line). In the presence of the magnetic field B , the single-electron state undergoes Zeeman splitting indicated by the two solid lines at energies $E_T \pm 1/2E_Z$. At low temperatures and high fields, only the lower spin state is occupied. If the Fermi level is raised, an additional electron from the channel can tunnel into the upper spin state in Fig. 4b, forming a two-electron singlet state (e.g., a lone pair). Thus, the Fermi energy required for forming the two-electron state would increase when B is increased, as suggested by Fig. 4a. In contrast, an initially “spinless” empty trap would fill the lower Zeeman level, producing the opposite field dependence (i.e., the required Fermi energy decreases with increasing B), contrary to observation. Therefore, the initial empty trap begins in a $1e$ paramagnetic state ($S = 1/2$) (high current state) while the filled trap (lower current state) is a $2e$ singlet state ($S = 0$).

The same statistical measurement approach can also be used to study the $2e$ singlet to $2e$ triplet transition. In the case when there is more than one orbital available in the trap, there is also a possibility of forming a triplet two-particle state. For sufficiently strong magnetic fields, the triplet energy will become lower than the singlet discussed above. For a singlet state, the trapping probability increases as B increases. In contrast, for the triplet state, the trapping probability decreases as B increases. In fact, such a signature has been seen for a couple of devices when they were cooled to cryogenic temperatures rapidly. The consequence of such a transition has been realized recently at high magnetic fields in a similar MOSFET system [10].

2.2 Detection of Electron-Spin Resonance (ESR) of a Single Spin

To perform gate operations of spin rotations, many existing techniques for magnetic spin resonance can, in principle, be used. However, it has generally been accepted that qubits should be represented as individual spins. So in order to manipulate individual spin qubits, one has to be able to at least monitor the electron-spin resonance (ESR) of a single spin. In recent years, there have been several examples [11–14] of detection of magnetic resonance on single-electron spins in solids. Spin resonance of the nitrogen-vacancy defect center in diamond was detected optically [11, 12]. Spin precession of a localized electron spin on a surface has been detected by scanning tunneling microscopy [13, 14].

To create spin resonance of the paramagnetic trap, microwave radiation from 16 to 26 GHz, is delivered by semirigid coaxial cable, to a coaxial-to-waveguide converter, inside a cryostat. For higher frequencies, 26.5 to 50 GHz, a rectangular waveguide is used as the transmission line. In both cases, the sample is mounted on an endplate of the waveguide where the magnetic-field component is maximum while the electric-field component is nearly zero. Eliminating the electric component of the microwave is critical for the measurement. The photoconductivity of the sample is normally minimized to a few per cent. An excessive amount of microwave electric field can cause spurious effects [15, 16].

Our ESR detection scheme is based on the changing balance between the two source/drain current states of the transistor, when the Larmor precession frequency produces spin-flips. In effect, this is transistor-current-detected ESR. Following the paramagnetic trap model, described by the energy-band diagram in Fig. 4b, one can imagine that when the microwave frequency is E_z/h (i.e., at spin resonance), the spin state can be flipped, as in Fig. 4c. When the paramagnetic spin flips, the lower Zeeman level becomes available for trapping an additional electron. The trapping event increases the average source/drain current. A rate equation analysis of this trap/channel configuration can be used to calculate the ESR-induced change in trap-filling probability [17]. To detect the ESR microwave-induced change, we measure channel current at a fixed microwave frequency for 300 ms, during which there are about a few thousand RTS switching events, giving good statistics for the RTS.

Figure 5a represents a fragment of such a trace over a 10-ms time interval. To complete the current versus magnetic field dependence, full 300-ms traces are taken at 150–250 different magnetic fields. Since the signals are sometimes noisy, a systematic statistical procedure was used to measure the trap charge state, as described in the last section. A histogram of the source/drain current data versus time, as shown in Fig. 3 is used to measure the statistics of both the empty and filled trap states represented by the two peaks. For the perfect case of two discrete states, one expects two delta functions in the histogram. The broadening of the peaks in Fig. 3 is caused by noise.

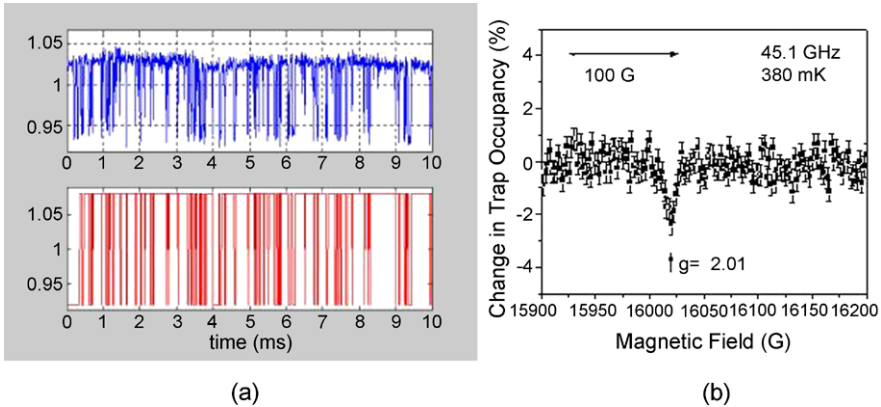


Fig. 5. (a) *Top*: the raw random telegraph data displayed for a time interval of 10 ms. *Bottom*: an algorithm for detection of abrupt changes is used on the raw data to reconstructed two-level RTS. This procedure reduces the statistical errors due to noise. (b) The change in trap-occupancy probability versus magnetic field for a fixed microwave frequency. The dip represents the electron-spin resonance

The charge-trapping probability ratio is proportional to the area ratio of the two peaks. For certain traps, whose charge produces only a small change in source/drain channel current, an additional step is taken to avoid noise errors. A more sophisticated algorithm [18], for detection of abrupt step changes, is executed numerically. As an example, the top of Fig. 5a is the raw random telegraph signal, containing noise. The bottom of Fig. 5a shows the noiseless two-state switching, reconstructed by the algorithm.

Figure 5b presents the ESR detection results for the single paramagnetic trap at a microwave frequency of 45.1 GHz. The error bars (about 1 per cent) in the figure indicate the standard deviation in a 300-ms dataset averaged over 4 adjacent magnetic fields. In Fig. 4a, an ESR peak in average current is centered around 16,025 G. Averaging blocks of 4 adjacent magnetic fields, the signal-to-noise ratio is greater than 4:1, and the ESR feature is reproducible in different runs, and for different traps, in different samples. The key to positively identify the single-trap ESR is from the change of RTS statistics rather than from device electrical conductance as it can drift with time and can be changed due to spurious effects [15, 16] induced by both electric and magnetic field components of the microwave. We find that the ESR signal is most pronounced in the range of gate voltages corresponding to a paramagnetic (nearly empty) trap (i.e., between points B and C in Fig. 2a). This is consistent with our assignment of filled and empty trap states. The ESR signature is only found at temperatures below about 1 K. At those temperatures, the electron magnetic moment is substantially polarized, and in any case, microwave heating limits the temperature. From the RTS Boltzmann occupation probability as a function of voltage, we find the effective tem-

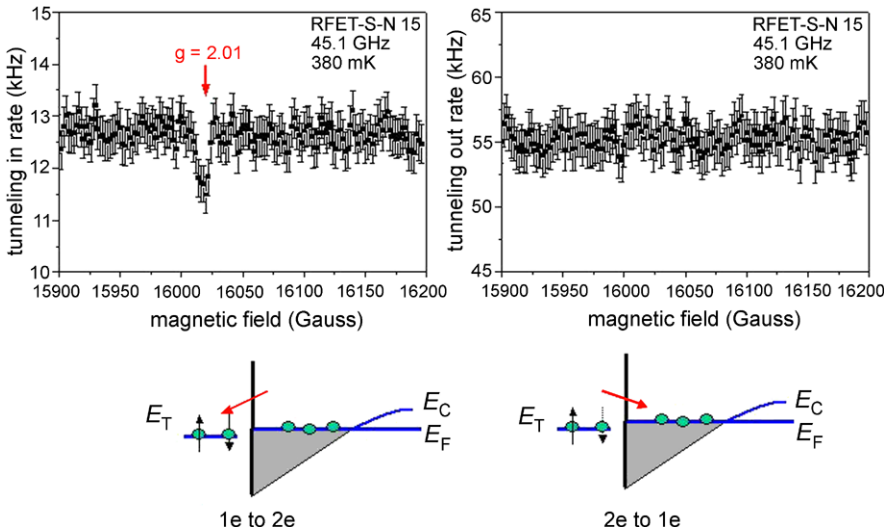


Fig. 6. The tunneling frequency is plotted as a function of magnetic field. While the rate of tunneling into the trap is substantially modified at ESR, the rate of tunneling out is unaffected by the ESR

perature rises to about 1 K when a moderate microwave power of 0.1 mW is applied to the sample, even though the bath temperature still remains at about 0.4 K [9].

Similar runs have been carried out at other frequencies and in various samples [19]. A g -factor of 2.02 ± 0.015 is obtained. Since conduction electrons always have $g \leq 2$, and paramagnetic centers in SiO_2 always have $g \geq 2$, our results indicate a paramagnetic center in the oxide, or at the SiO_2/Si interface. Our observed g -value is somewhat larger than that for some known paramagnetic centers near the interface.² A P_b center is known to have a g -factor of 2.006 along the $\langle 100 \rangle$ direction, while the E' center is expected to have $g = 2.0005$. One possibility is that we are looking at a center that has a different local structure from these two typical examples. Another possibility is that the low-density conduction channel electrons might have slight ferromagnetic ordering, giving rise to a local field that slightly increases the apparent g -factor of the trap. We found that the large Rabi frequency produces nonlinear effects. At lower radio powers the trapping probability increases at ESR, and a peak is expected [17]. However, at higher powers, the ESR-induced signal inverts, leading to a decrease in trapping probability, as plotted in Fig. 5b.

We also see a nonlinear ESR response in the tunneling dynamics. In Fig. 6, the tunneling frequency is plotted as a function of field. While the rate of tunneling into the trap is substantially modified (about 10 per cent change) at

² See for example [20].

ESR, the rate of tunneling out is unaffected by the ESR. This observation is consistent with the fact that the $2e$ state is a singlet that should be insensitive to the spin-flip by ESR.

The detection of ESR of a single-spin trap was also reported by another group at a much higher temperature [21]. In their experiment, data was collected over a long period of time (\sim days) for a magnetic field scan at a fixed frequency.

2.3 Single-Shot Measurement

Although our group has been the first to electrically measure electron-spin resonance on a single semiconductor spin, due to the tiny difference in energy between the two spin states (limited by the low frequency in common commercial microwave generators) and the electronic heating generated by the continuous microwave radiation, the spin-orientation information was obtained by repeated measurements and thermal averaging. However, the method of spin orientation to charge conversion used for the ESR detection is completely compatible with single-shot read out (i.e., measuring two orthogonal spin states of the trap without repetition), required for quantum computation. The Fermi level can be adjusted so that it lies between the upper and lower Zeeman levels as illustrated in Fig. 4. At low temperatures and high B fields, if the lower Zeeman level is occupied by one electron, as in Fig. 4b, it cannot accept any additional electrons from the Fermi level. If only the upper Zeeman level is occupied, as in Fig. 4c, then an additional electron can be transferred from the Fermi sea to the lower Zeeman level. The distinction between two trapped charges, $2e$, versus one trapped charge, $1e$, can be sensed by the FET channel (i.e., the electrometer). For a practical quantum computer, the heating can be avoided by using microwave-free spin rotation for the single-qubit gates [1]. A similar spin-to-charge conversion scheme was, in fact, used to detect the spin orientation of a single spin in a GaAs quantum dot by a single tunneling event [22].

3 Fabrication and Characterization of Electrostatically Confined Quantum-Dot Structures in Si/SiGe Heterostructures

Although the single-spin measurements described in the previous section, were done on a structure that closely resembles nearly all proposed spin-based qubit architectures, the device uses a randomly positioned defect as its electron trap. It has been the goal of the community to fabricate similar devices in specially designed semiconductor structures that promise greater control over electron spin with the ability to entangle two spins, and to eventually build a scalable quantum processor.

Significant effort has been directed toward the development of electrostatically defined quantum dots as potential elements for quantum computation information. While a high level of control and sophistication has been achieved in current GaAs/AlGaAs-based structures [22–24], silicon-based heterostructures are expected to have the distinct advantage of possessing extremely long electron phase-coherence lifetimes, which can be attributed to the small spin-orbit interaction and the low natural abundance of isotopes with nuclear spin. Means of control in lateral quantum-dot devices is often exercised through the use of Schottky barrier top gates in which metal electrodes patterned on the semiconductor surface capacitively couple to the 2DEG. By applying a bias on the gates one can selectively deplete the charge carriers in the 2DEG directly below, and in the vicinity of the gates thereby controlling current flow.

Over the last several years attempts were made to create mesoscopic devices on strained Si/SiGe heterostructures by directly mimicking the existing geometries and fabrication processes that have been employed on GaAs/AlGaAs-based heterostructures. The success was often limited due to the high level of leakage current and/or the incomplete depletion of the 2DEG by Schottky gates on strained Si/SiGe. Several innovative approaches have recently been introduced as means of circumventing these obstacles. For example, Bo et al. [28] and Klein et al. [29] have fabricated quantum dots (QDs) by using atomic force microscope lithography and electron-beam lithography on Si/SiGe heterostructures, respectively. In their devices, trenches are created by the lithography, and the isolated two-dimensional electron regions are used as gates to control a QD surrounded by the trenches. Sakr et al. [30] of the UCLA group, has fabricated a laterally confined quantum-dot structure that is integrated with a charge readout channel using a strained Si layer on strain-relaxed SiGe buffer layers. In this structure, a new approach has been developed to embed leakage-secluded metallic side gates in etched grooves that provide stronger gate to quantum-dot coupling. Devices with different sizes show reproducible single-electron charging effects and are stable over an extended period of time for dots of 30–150 electrons. The discrete electronic occupation of the quantum dots can be effectively detected using the adjacent quantum point-contact electrometer.

3.1 Demonstration of a One-Electron Quantum Dot

As a result of the continuous technical improvement of the nanofabrication techniques as well as the quality of epitaxial materials, the UCLA group has recently fabricated another generation of devices that show unprecedented high quality in terms of device stability and degree of gate control. The second generation of devices used a low-temperature thermal oxidation process to grow a very thin oxide layer (about 3 nm) making use of the cap layer of the epitaxial wafer. The incorporation of this unconventional insulating layer

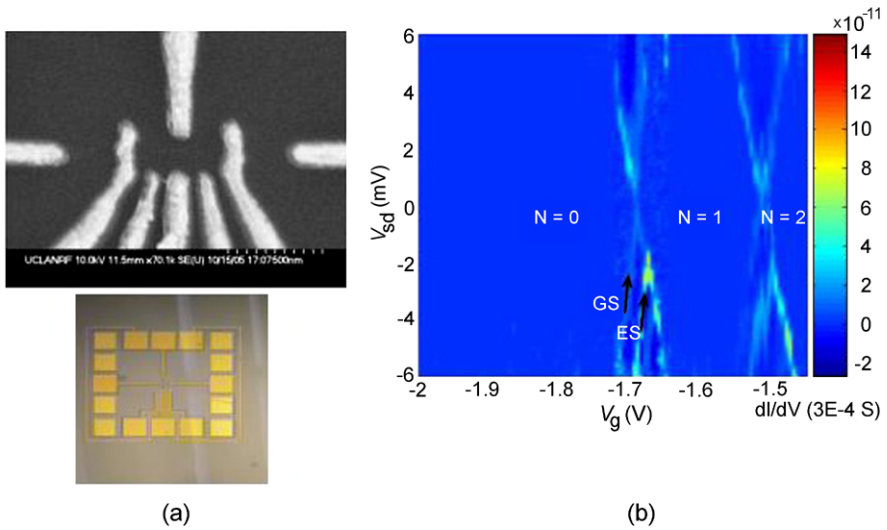


Fig. 7. (a) Scanning electron micrograph and electrode layout of the quantum-dot structure. (b) Stability plot of the differential conductance in a grayscale as a function of the source–drain voltage, V_{sd} , and the plunger gate voltage, V_g , at 0.4 K, completed in about 2 h

suppressed the gate leakage current to less than 0.1 pA at typical operation voltages.

Figure 7 shows two coupled quantum dots that are each defined by 4 gates. The layout of the device is adapted from what has been used successfully in GaAs/AlGaAs materials. As a result of the low leakage current the effective electron temperature is in equilibrium with the bath temperature and the conduction peaks are much narrower than that for the earlier-generation devices. Consequently, the stability diagram (i.e., dI/dV vs. V_{sd} vs. V_g shown in Fig. 7) reveals even the excited-state energy levels. More importantly, the insulating layer allowed us to pattern strongly coupled surface gates that were able to squeeze the number of electrons in the dot down to zero for the first time in SiGe-based quantum-dot devices. The complete absence of electrons in the dot at high gate voltages was verified by two well-established techniques. First, at high gate voltage there is no conductivity at sufficiently high source–drain bias. Second, the lowering of the tunneling barriers produced no additional conduction peaks. With the new generation of devices we can now vary the number of electrons in each dot precisely from 0 to 5 and change the effective interaction of the two dots. The stability plot measures the charging energy and the dot size. We found a charging energy of about 20 meV for the last observable Coulomb diamond. A dot diameter of about 20 nm can be deduced from this large charging energy.

With this new generation of structure, the spin splitting is also clearly visible in the stability diagram at high fields, as shown in Figs. 8a and b.

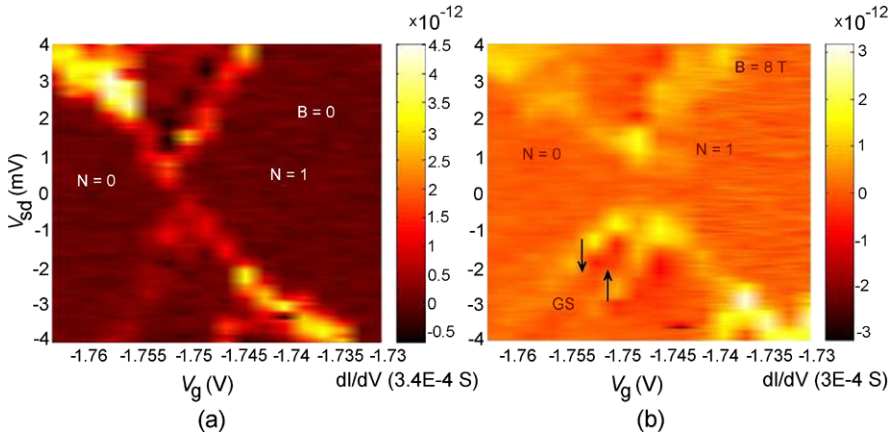


Fig. 8. The stability diagram at (a) $B = 0$ T and (b) at $B = 8$ T, the spin splitting is clearly visible as labeled by the two arrows

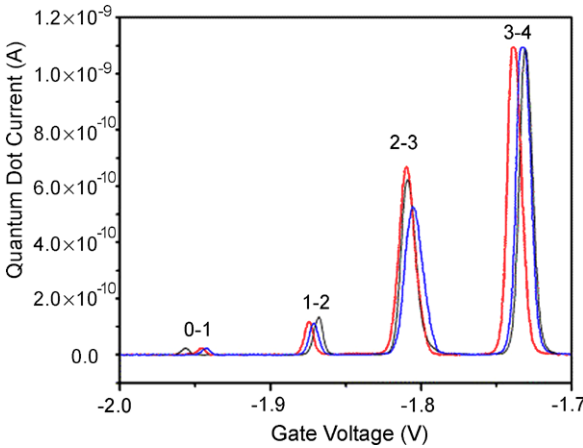


Fig. 9. Several successive traces of channel current as a function of gate voltage under the same conditions. Slight shifts in peak positions can be seen for different scans indicating long-term electric instability

Despite these encouraging developments, the surface gates on an oxide can often produce unexpected charges in the vicinity of the dots that alter the confinement potential and produce $1/f$ noise that affect the long-term electronic stability. For example, Fig. 9 shows several successive scans of channel current as a function of gate voltage under the same conditions. Slight shifts in peak positions can be seen for different scans. The fuzziness of the boundary lines in the stability diagram in Fig. 8 is another manifestation of the electric instability. This slight shift can make a pump/probe study, like that performed in GaAs systems, impossible. We also noticed that for the multiple gates, a couple of gates were dominant in the formation of the dot. We believe the un-ionized donor impurities can play important roles on small scales for the depletion-mode quantum dots.

In order to further utilize these Si devices for quantum information processing experiments including precise pulse-controlled spin logic and high-bandwidth readouts, the electrostatic environment has to be stable during the period of experiments. Towards this end, both Berer et al. [31] and Slinker et al. [32] have successfully used evaporated Pd on strained Si/SiGe as Schottky gates. Despite these hopeful results, it is recognized that further improvement of the effectiveness of the Schottky gates is needed to gain ultimate control in the few-electron regime.

In a more recent development, Scott et al. of the UCLA group came up with a new innovation that can produce high-quality Schottky gates for strained Si/SiGe heterojunctions, capable of depleting the high-mobility two-dimensional electrons locally, possessing superb leakage properties. We found that gold sputtered in Ar plasma forms an excellent Schottky gate. The surface gate depletes the underlying electrons at a small negative bias, which demonstrates that there are small numbers of surface states. The sputtered gold gates always showed dramatically less leakage current as compared to the evaporated gates [25]. In fact, the leakage current was at least five orders of magnitude lower compared to Au gates deposited by evaporation. We believe the surprisingly effective sputtered Au gates is a result of the interdiffusion of gold and SiGe atoms initiated by the energetic plasma gas. The Schottky barrier is likely a gold silicide compound, similar to the well-known platinum silicide, which is now used reliably with CCD camera production. To implement the sputtered Au process as surface gates at submicrometer scales, we have developed a so-called dual-layer process, which combines sputtering and evaporation and is compatible with standard electron-beam lithography. Because this technique is relatively simple and enables the formation of devices with conventional surface gates, it may be more readily incorporated into components for qubit applications.

3.2 Characterization of the Spin-Transition Sequence

With the MOSFET-like quantum-dot devices, we have performed an experiment to determine the spin transitions in the few-electron regime since the information is critical to design logic operations as well as readout steps. The energy of the conduction peaks (i.e., the Coulomb-blockade peaks) is measured as a function of the inplane magnetic field. The peak position depends on the magnetic field, B , through the Zeeman term, $-g\mu_B[S_z(N+1) - S_z(N)]$. The reason to apply an inplane field rather than a normal field is that we are interested mainly in the spin characteristics of the trap and would like to minimize the effects due to the orbital motion of electrons in the quantum dot. The field dependence gives information about the z -component of the quantum-dot spin. The negative slope of the line in the peak position vs. field curve indicates that the spin is added parallel to B . The energy shift can be readily calculated from the gate-voltage shift using the ratio of the horizontal to vertical scale in the stability diagram. We have discovered an unexpected

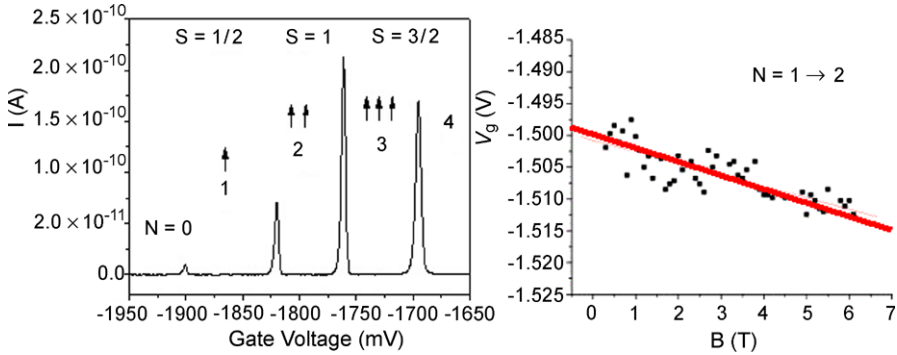


Fig. 10. (a) The channel current as a function of gate voltage at a fixed magnetic field. The transitions between different charge states have been labeled. (b) The Coulomb-blockade peak for the $1e$ to $2e$ transition as a function of the inplane magnetic field

spin-transition sequence as the number of electrons changed from 1 to 3. The total spins of the dot were found to be $S(N = 1) = 1/2$, $S(N = 2) = 1$, and $S(N = 3) = 3/2$. This sequence is very different from that in a GaAs quantum dot, which was expected to have a $1/2$ to 0 to $1/2$ order. We believe the unusual configuration is most likely due to the electron–electron correlations in the dot [26]. Because of the large effective electron mass, the interaction energy becomes larger than that of the single-electron level spacing. So, the electrons prefer to occupy the high-energy levels to gain the exchange energy. Similar observations of high-spin states have been reported earlier in an etched Si dot fabricated from a Si-on-insulator wafer [27].

3.3 Single-Shot Measurement

As discussed earlier, for a practical operation of readout, one has to complete the measurement in a single attempt with high reliability. More specifically, one has to be able to measure two orthogonal spin states of the trap without repetition (i.e., single-shot). We would like to describe here schematically the procedures for such a measurement in the quantum-dot case.

The spin in the quantum dot is initially prepared in the “ground” (spin-up) state. This initialization can be done by first raising the Fermi level between the two spin states such that the spin-up state of the empty dot can be filled. The Fermi level is then raised slightly above the spin-down state. Since it takes a large charging energy to add the second electron, the down-spin state is guaranteed to be empty as shown in Fig. 11a. Instead of applying continuous microwave radiation, one can apply a short pulse that puts the trapped spin into a superposition of spin-up and spin-down states, as in Fig. 11b. This step is equivalent to a single qubit rotation. Next, one can apply a voltage to the gate to shift the Zeeman doublet to the config-

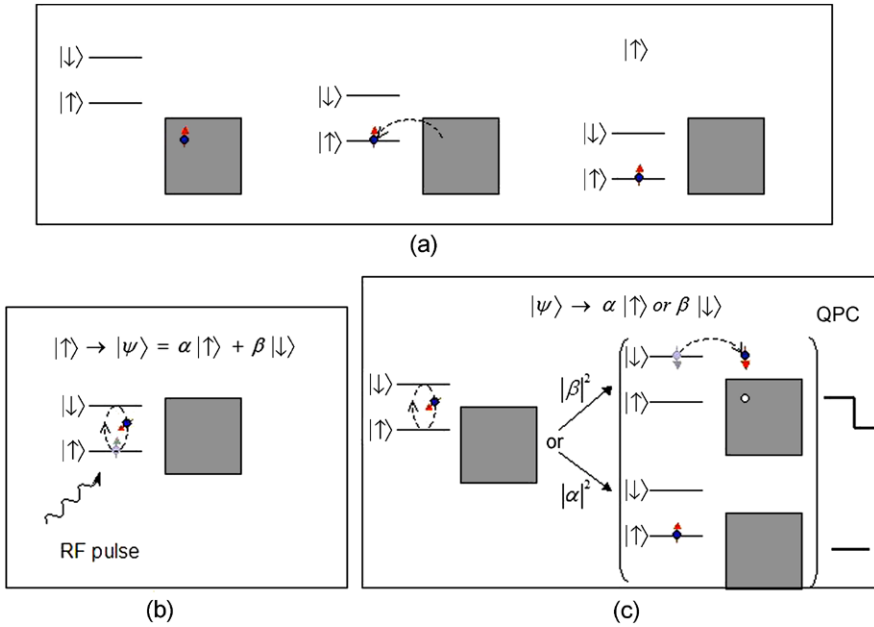


Fig. 11. Schematics for single-shot spin-state readout: (a) The spin-state initialization, (b) The spin state is prepared in a superposition by a microwave pulse, and (c) The state is then measured by detecting (or not detecting) the current jump in the QPC signal

uration shown in Fig. 11c. The spin-down state tunnels out (provided the spin-relaxation time T_1 exceeds the trapped-electron dwell time), while tunneling of the spin-up state is prohibited by the exclusion principle for a singlet state. Thus, the transport current will exhibit a jump, which can be associated with the spin-down state. What happens, if the electron is a superposition of spin-up and spin-down states? In this case, repetitive measurements using the same pulsewidth can obtain the superposition coefficients α and β . A systematic measurement as a function of the pulsewidth will provide one with the Rabi oscillation frequency that will precisely calibrate the gate operation timing. Inducement and control of coherent coupling between different qubits is a central issue in any architecture for quantum information processing. We would like to point out that the true quantum measurement described here is fundamentally different from the ensemble measurement that was already performed successfully in the GaAs quantum-dot system [33], where a probing current is passed through the dot. We believe that the capability to conduct the true quantum measurements of a single-spin state will be a major advancement in science and a significant step towards the physical implementation of spin-based quantum information processing.

4 Concluding Remarks

In conclusion, the research of individual-spin-based quantum information processing in Si materials has made remarkable progress in the last several years. The advancement can be summarized in two areas. First, manipulation and detection of an individual single-electron spin is now becoming reality by successfully implementing spin to charge conversion. Secondly, continuous effort and technological progress now allow us access to the few- and single-electron spin regimes in strained Si/SiGe epitaxial structures, which was not possible only a few years ago. The quality and stability of the engineered quantum-dot structures in strained SiGe are now catching up to the more mature GaAs-based quantum-dot structures. We believe that quantum information processing based on the individual electron spins in Si has distinct advantages over other competing physical systems, and will have a bright future through sustained research and development efforts.

Acknowledgements

We would like to express our gratitude to Dr. Ivar Martin of Los Alamos National Laboratory for theoretical support to the project, and Prof. Kang Wang for helping to secure the Si FET samples. The research at UCLA was supported by the Defense Advanced Research Projects Agency, and the Defense MicroElectronics Activity.

References

1. E. Yablonovitch, H.W. Jiang, H. Kosaka, H. Robinson, D. Sethu Rao, T. Szkopek, *Proc. IEEE* **91**, 727 (2003). Special Issue on Spintronics Technology 81, 91
2. B.E. Kane, *Nature* **393**, 133–137 (1998) 82
3. A.M. Tyryshkin, S.A. Lyon, A.V. Astashkin, A.M. Raitsimring, *Phys. Rev. B* **68**, 193207 (2003) 82
4. R. Vrijen, E. Yablonovitch, K. Wang, H.W. Jiang, A. Balandin, V. Roychowdhury, T. Mor, D. DiVincenzo, *Phys. Rev. A* **62**, 12306 (2000) 82
5. D. Loss, D.P. DiVincenzo, *Phys. Rev. A* **57**, 120 (1998) 82
6. M. Friesen, P. Rugheimer, D. Savage, M.G. Lagally, D.W. van der Weide, R. Joynt, M. Eriksson, *Phys. Rev. B* **67**, 121301 (2003) 82
7. M.J. Kirton, M.J. Uren, *Adv. Phys.* **38**, 367–408 (1989) 84
8. K.S. Ralls, W.J. Skocpol, L.D. Jackel, R.E. Howard, L.A. Fetter, R.W. Epworth, D.M. Tennant, *Phys. Rev. Lett.* **52**, 228–231 (1984) 84
9. M. Xiao, I. Martin, H.W. Jiang, *Phys. Rev. Lett.* **91**, 18301 (2003) 84, 86, 90
10. E. Prati, M. Fanciulli, G. Ferrari, M. Sampietro, *Phys. Rev. B* **74**, 033309 (2006) 87

11. J. Khler, J.A.J.M. Disselhorst, M.C.J.M. Donckers, E.J.J. Groenen, J. Schmidtand, W.E. Moerner, *Nature* **363**, 242–244 (1993) 88
12. F. Jelezko, T. Gaebel, I. Popa, A. Gruber, J. Wrachtrup, *Phys. Rev. Lett.* **92**, 076401 (2004) 88
13. Y. Manassen, R.J. Hames, J.E. Demuth, A.J. Castellano, *Phys. Rev. Lett.* **62**, 2531 (1989) 88
14. C. Durkan, M.E. Welland, *Appl. Phys. Lett.* **80**, 459 (2002) 88
15. E. Prati, M. Fanciulli, A. Calderoni, G. Ferrari, M. Sampietro, *Phys. Lett. A* **370**, 491–493 (2007) 88, 89
16. E. Prati, M. Fanciulli, A. Calderoni, G. Ferrari, M. Sampietro, *J. Appl. Phys.* **103**, 104503 (2008) 88, 89
17. I. Martin, D. Mozysky, H.W. Jiang, *Phys. Rev. Lett.* **90**, 018301 (2003) 88, 90
18. W. Liu, Z. Ji, L. Pfeiffer, K.W. West, A.J. Rimberg, *Nature* **423**, 422 (2003) 89
19. M. Xiao, I. Martin, E. Yablonovitch, H.W. Jiang, *Nature* **430**, 435 (2004) 90
20. E.H. Poindexter, in *Semiconductor Interfaces, Microstructure, and Devices* (Institute of Physics, Bristol, 1993) 90
21. M.S. Brandt, S.T.B. Goennenwein, T. Graf, H. Huebl, S. Lauterbach, M. Stutzmann, *Phys. Status Solidi* **8**, 2056 (2004) 91
22. J.M. Elzerman, R. Hanson, L.H. Willems van Beveren, B. Witkamp, L.M.K. Vandersypen, L.P. Kouwenhoven, *Nature* **430**, 431 (2004) 91, 92
23. N.J. Craig, J.M. Taylor, E.A. Lester, C.M. Marcus, M.P. Hanson, A.C. Gossard, *Science* **304**, 565 (2004) 92
24. J.R. Petta et al., *Science* **309**, 2180 (2005) 92
25. G.D. Scott, M. Xiao, E.T. Croke, E. Yablonovitch, H.W. Jiang, *Appl. Phys. Lett.* **90**, 032110 (2007) 95
26. Y. Hada, M. Eto, *Phys. Rev. B* **68**, 155322 (2003) 96
27. L.P. Rokhinson, L.J. Guo, S.Y. Chou, D.C. Tsui, *Phys. Rev. B* **63**, 035321 (2001) 96
28. X.Z. Bo, L.P. Rokhinson, H. Yin, D.C. Tsui, J.C. Sturm, *Appl. Phys. Lett.* **81**, 3263 (2002) 92
29. L.J. Klein, K.A. Slinker, J.L. Truitt, S. Goswami, K.L.M. Lewish, S.N. Coppersmith, D.W. van der Weide, M. Friesen, R.H. Blick, D.E. Savage, M.G. Lagally, C. Tahan, R. Joynt, M.A. Eriksson, J.O. Chu, J.A. Ott, P.M. Mooney, *Appl. Phys. Lett.* **84**, 4047 (2004) 92
30. M.R. Sakr, E. Yablonovitch, E.T. Croke, H.W. Jiang, *Appl. Phys. Lett.* **87**, 223104 (2005) 92
31. T. Berer, D. Pachinger, G. Pillwein, M. Muhlberger, H. Lichtenberger, G. Brunthaler, F. Schaffler, [arXiv:cond-mat/0508260](https://arxiv.org/abs/cond-mat/0508260) (2005) 95
32. K.A. Slinker, K.L.M. Lewis, C.C. Haselby, S. Goswami, L.J. Klein, J.O. Chu, S.N. Coppersmith, R. Joynt, R.H. Blick, M. Friesen, M.A. Eriksson, [arXiv/0508107](https://arxiv.org/abs/0508107) (2005) 95
33. F.H.L. Koppens et al., *Nature* **442**, 766 (2006) 97

Index

conversion, 91

pump/probe, 94

quantum information processing, 82, 97

quantum information processor, 81, 82

random telegraph signal, 83

readout channel, 92

Si/SiGe heterostructure, 92

single-shot read out, 91

spin resonance, 89

spin-to-charge, 91